Editors' Suggestion | Featured in Physics

Observation of Vinen Turbulence During Far-from-Equilibrium Bose-Einstein Condensation

Sebastian J. Morris,* Martin Gazo, Simon M. Fischer, Haoyu Zhang, Christopher J. Ho,†
Nigel R. Cooper, Christoph Eigen, and Zoran Hadzibabic
Cavendish Laboratory, University of Cambridge, J. J. Thomson Avenue, Cambridge CB3 0US, United Kingdom

(Received 8 May 2026; revised 25 June 2026; accepted 10 September 2026; published 5 November 2026)

Relaxation of far-from-equilibrium quantum fluids, intimately related to the emergence of long-range order, is theoretically associated with the decay of a turbulent isotropic tangle of vortex lines. We observe and study such decaying quantum turbulence in a homogeneous 3D atomic Bose gas. Using matter-wave techniques to magnify the gas density distribution, and then imaging a thin slice of the magnified cloud, we observe imprints of randomly oriented vortex lines and measure the vortex-line-length density $\mathcal{L}$. The observed decay of $\mathcal{L}$ agrees with the prediction for Vinen "ultraquantum" turbulence. Although our weakly interacting gases are highly compressible, their large-scale dynamics are consistent with the behavior of an incompressible hydrodynamic fluid, with the decay of $\mathcal{L}$ not depending on the strength of the interatomic interactions and being similar to that in the strongly interacting superfluid helium.

DOI: 10.1103/lywd-gjg9

A striking feature of quantum fluids is their irrotational flow, which leads to a quantized circulation that establishes topological defects in the form of vortex lines [1–4]. The interactions and reconnections of quantized vortices are at the heart of a rich phenomenology of far-from-equilibrium dynamics, relevant across many fields and length scales [5–11]. Central to these dynamics is the phenomenon of quantum turbulence, which has long been a cornerstone of research in superfluid helium [12–16].

The regime of Vinen or ultraquantum turbulence [13,16] corresponds to the decay of a random vortex tangle [see Fig. 1(a)] without any large-scale (classical) flow. Such turbulence has been theoretically linked to the dynamics of Kibble's strings in cosmology [8] and predicted to play a key role in far-from-equilibrium Bose-Einstein condensation (the emergence of long-range coherence) [24–30]. Quantitatively, it is characterized by the vortex-line-length density $\mathcal{L}$, i.e., the total length of vortex lines per unit volume. In liquid helium, the decay of $\mathcal{L}$ has been measured indirectly, using sound attenuation, already 70 years ago [5,6]. In this case, up to possible logarithmic corrections,

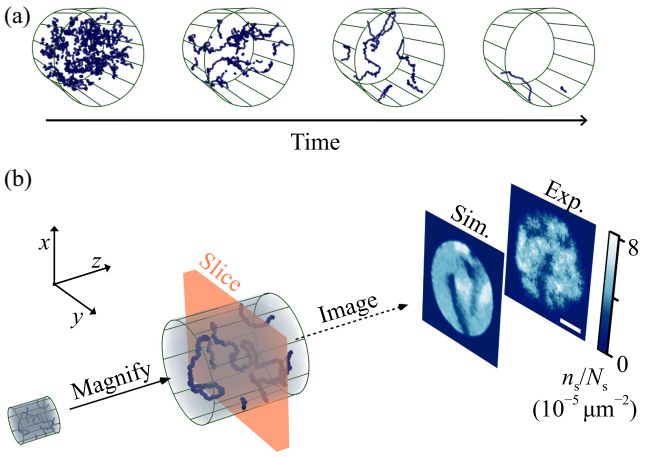


FIG. 1. Detecting decaying quantum turbulence during far-from-equilibrium condensation in an isolated gas. (a) Cartoon of the expected vortex-tangle decay; the cylindrical container shows the geometry of our optical box trap [17,18]. (b) Experimental concept. We magnify the cloud [19–21] (by a factor of ≈3.5 in the x-y plane) and then image just a slice of it (orange shading) [22], so the imprints of the random vortex lines (dark lines) start and stop as they enter and leave the imaged slice. We show an experimental image and a numerical simulation with similar parameters. Here n_s is the imaged 2D density, N_s is the total number of imaged atoms, and the scale bar shows 50 μm. Our box trap has volume $V \approx 9 \times 10^4$ μm^3, the gas has density $n \approx 2.2$ μm^{-3}, and the *in situ* vortex-core size is set by the healing length $\xi \sim 1$ μm; theoretically, the FWHM of the density dip associated with a vortex is $\approx 3\xi$ [23]. The thickness of the imaged slice and the apparent vortex-line diameter are both ≈15 μm; the latter is consistent with our magnification procedure and imaging resolution of ≈5 μm.

*Contact author: sm2357@cam.ac.uk
†Present address: Centre for Cold Matter, Blackett Laboratory, Imperial College London, Prince Consort Road, London SW7 2AZ, United Kingdom.

Published by the American Physical Society under the terms of the Creative Commons Attribution 4.0 International license. Further distribution of this work must maintain attribution to the author(s) and the published article's title, journal citation, and DOI.

$$\frac{d\mathcal{L}}{dt} = -B\mathcal{L}^2, \tag{1}$$

where B is a constant with units of the quantum of circulation, $2\pi\hbar/m$, with m being the particle mass [13,25]. Individual vortex lines have also been visualized using tracer particles, but such tracers are large compared to the vortex core and can modify the vortex dynamics [31–34].

Ultracold atomic gases provide an excellent setting for studies of both driven and freely decaying turbulence [35–51]. In many situations, these systems also allow direct imaging of vortices [35,37,39–41,43,46,52–64], but a quantitative study of isotropic 3D vortex tangles has remained a challenge. Recently, a study of far-from-equilibrium condensation in a homogeneous gas [50] revealed dynamics of the coherence length ℓ consistent with Eq. (1), assuming that ℓ is set by the typical vortex-line separation [13], so $\ell \propto \mathcal{L}^{-1/2}$. This study was based on measurements of the gas momentum distribution, which is sensitive to the presence of vortices but does not directly reveal them, and the observed dynamics of ℓ were also consistent with wave-based theories [65–68].

In this Letter, we directly observe Vinen turbulence, during far-from-equilibrium condensation in a homogeneous 3D atomic gas. To reveal imprints of the randomly oriented vortex lines, we magnify the cloud [19–21] and then image just a thin slice of it [22]; see Fig. 1(b). We measure the vortex-line-length density $\mathcal{L}$, observe a nonlinear decay of $\mathcal{L}$ in accordance with Eq. (1), and show that the prefactor B does not depend on the strength of the (weak) interparticle interactions. As in the strongly interacting superfluid helium [69], we find $B \approx \hbar/m$.

In our experiments, we prepare an isolated Bose gas in a far-from-equilibrium initial state by starting with a Bose-Einstein condensate and then perturbing it, as in Refs. [50,70]. Our ^{39}K gas is in the lowest hyperfine state, trapped in a cylindrical optical box [17,18] of volume $V \approx 9 \times 10^4$ μm^3 [diameter 47(2) μm and length 52(2) μm], and has density $n \approx 2.2$ μm^{-3}, corresponding to the critical temperature for condensation $T_c \approx 70$ nK. The initial state is incoherent but low energy, with energy per particle $\approx k_B \times 20$ nK, corresponding to the equilibrium condensed fraction $\eta \approx 0.5$ [50]. We tune the interactions in the gas, characterized by the s-wave scattering length a, using the Feshbach resonance at 402.7 G [71]; the initial incoherent state is prepared at $a = 0$ [72] and we initiate the gas relaxation by turning on the interactions, at time $t = 0$. In the interacting gas, the (equilibrium) radius of the vortex-line core is set by the healing length, $\xi = 1/\sqrt{8\pi n a}$, of order 1 μm.

To observe vortex imprints, we switch off the box trap and the interactions ($a \to 0$) and magnify the cloud [19–21] in the x-y plane by a factor $M \approx 3.5$ [see Fig. 1(b)]; as in Refs. [19–21,73–75], we use a pulsed harmonic potential as a matter-wave lens [76]. We then image just a central slice of the cloud [22], of thickness $d \approx 15$ μm [77]. The vortex lines that cross this slice appear as high-contrast dips (dark lines) in the imaged 2D density n_s. Theoretically, the *in situ* FWHM of the density depletion due to a vortex core is $\approx 3\xi$ [23], while the apparent vortex-core diameter in our images (≈ 15 μm) is slightly larger than $3M\xi$, both due to our imaging resolution (≈ 5 μm) and because the free expansion along z during the 19 ms of x-y magnification leads to some blurring.

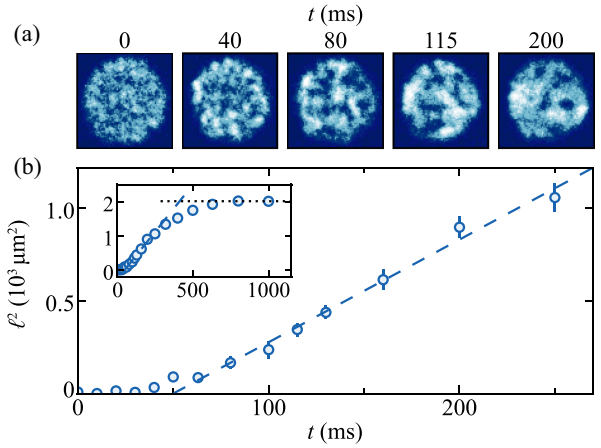


FIG. 2. Stages of relaxation, starting in an incoherent state. Here the scattering length is $a = 430a_0$, so $\xi = 0.9$ μm. (a) Examples of cloud slices at different relaxation times, imaged in separate experimental runs; the scale bar and the color scale are the same as in Fig. 1(b). The early-time images show only small-scale density fluctuations, whereas for $t \gtrsim 80$ ms we observe well-defined and well-separated vortex lines. (b) The corresponding evolution of the coherence length ℓ, obtained from separate measurements of momentum distributions, as in Ref. [50]. We find that the onset of universal coarsening seen in $\ell^2(t)$, given by $d\ell^2/dt \approx 3.4\hbar/m$ (dashed line) [50], and the emergence of well-defined vortices essentially coincide. The inset shows how $\ell^2(t)$ saturates at longer times; the dotted line shows $V^{2/3}$.

In Fig. 2(a), we show characteristic slice images for different relaxation times, with a set to $430a_0$ (where a_0 is the Bohr radius). At early times, we observe only small-scale density fluctuations, while at long times (here $t \gtrsim 80$ ms) we observe well-defined and well-separated vortex imprints.

For comparison, in Fig. 2(b) we show the corresponding evolution of $\ell^2(t)$, which shows universal coarsening, given by $d\ell^2/dt \approx 3.4\hbar/m$ [50], once ℓ significantly exceeds ξ and until it becomes comparable to the system size; as in Ref. [50], we obtain $\ell(t)$ from momentum-distribution measurements and normalize it such that $\ell^3 = V$ for an equilibrium condensate.

This comparison shows that the emergence of well-defined vortices essentially coincides with the onset of the universal coarsening seen in $\ell^2(t)$. Such coarsening does not directly reveal vortices, but is indeed consistent with the

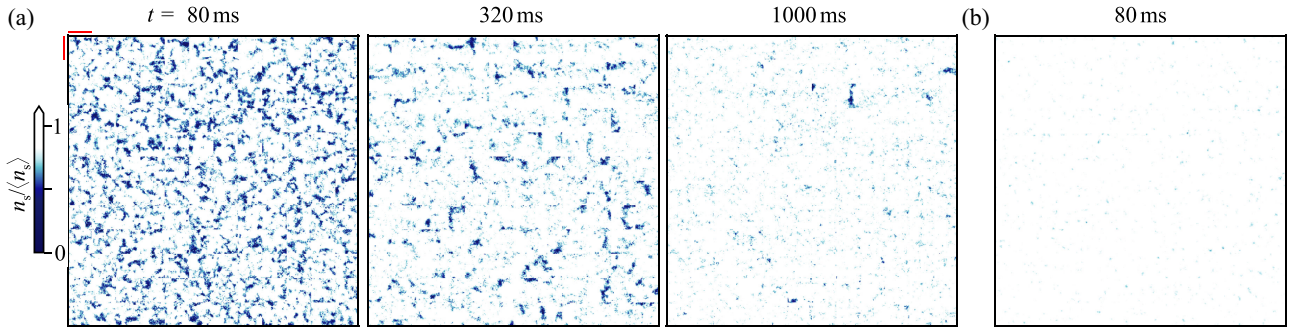


FIG. 3. Visualizing the decay of vortex lines. (a) For $t \geq 80$ ms, when vortices are well defined (see Fig. 2), we tile cropped slice images corresponding to 12×12 consecutive experimental realizations, which show randomly varying vortex configurations. The red bars in the top-left corner indicate the size of a single-image tile, which corresponds to $\approx 30 \times 30$ μm^2 *in situ*, and $\langle n_s \rangle$ is the average over the experimental repetitions. (b) Here, for $t = 80$ ms, we tile images taken without slicing (i.e., with line-of-sight integration over the whole magnified cloud). In this case, with the same color scale as in (a), no vortex imprints are observed.

Vinen scenario of well-separated vortex lines, with $\ell^2 \sim 1/\mathcal{L}$ [13,16]. It is also consistent with the notion that at length scales $\gg \xi$ the gas is effectively incompressible [65], similar to the effective incompressibility of classical gases for Mach numbers $\ll 1$ [78].

The long-time vortex configurations for fixed t vary randomly between experimental realizations, but statistically the number of vortex imprints decays. We illustrate this in Fig. 3(a) for $t \geq 80$ ms. Here, for each t, we tile 12×12 consecutively taken images, cropped to the central square area corresponding to $\approx 30 \times 30$ μm^2 *in situ* ($\approx 100 \times 100$ μm^2 after magnification). At times significantly beyond $t = 320$ ms, vortex imprints appear in a small fraction of experimental realizations; as our tiling visually suggests, in a much larger system their typical separation would be larger than our system size. For comparison, in Fig. 3(b) we show that if we image the whole cloud, instead of just a slice, no vortex imprints are observed.

For the quantitative analysis of our data, we employ the general mathematical result for an isotropic random tangle of lines [79],

$$\mathcal{L} = 4N_i/S, \tag{2}$$

where N_i is the number of intersections of lines with a subvolume of surface area S. In our case, N_i is the number of distinct vortex imprints, and S is the *in situ* surface area corresponding to the region where we count them [80].

We define the image area covered by the imprints by $n_s < \alpha \langle n_s \rangle$, where $\langle n_s \rangle$ is the average n_s, and set the cutoff $\alpha = 0.5$ to capture the high-contrast depletions associated with the vortices while excluding other density variations (including noise). We then count N_i by grouping the imprint pixels into the same cluster when they are separated by ≤ 4 pixels ≈ 10 μm [81].

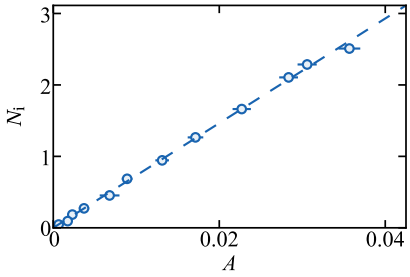


FIG. 4. Counting distinct vortex imprints. As expected, the average number N_i of distinct vortex imprints counted by our algorithm is proportional to the average fractional area A that they cover [see Fig. 3(a)].

More intuitively, $\mathcal{L}$ is proportional to the average fractional area A covered by the imprints: $\mathcal{L} \approx A/(wd)$, where w is the average imprint width. We show in Fig. 4 that our N_i, and hence $\mathcal{L}$ extracted according to Eq. (2), is indeed proportional to A. Then, Eq. (2) provides an absolute calibration of $\mathcal{L}/A$ in a way that does not depend on the vortex-core size and allows direct comparison of the dynamics at different a [82].

In Fig. 5(a), we plot the extracted $\mathcal{L}(t)$ for $a = 430a_0$ and $t > 80$ ms. At very long times (very small $\mathcal{L}$), the data are described well by a simple exponential decay (dashed line), with a time constant ≈300 ms; such one-body decay is suggestive of individual vortices annihilating on the trap walls with their images [83]. However, at earlier times we observe a decay faster than the exponential one, which we attribute to the vortex-vortex interactions that drive Vinen turbulence. Augmenting Eq. (1) to include one-body decay, we have

$$\frac{d\mathcal{L}}{dt} = -B\mathcal{L}^2 - \frac{\mathcal{L}}{\tau}, \tag{3}$$

which after integration gives

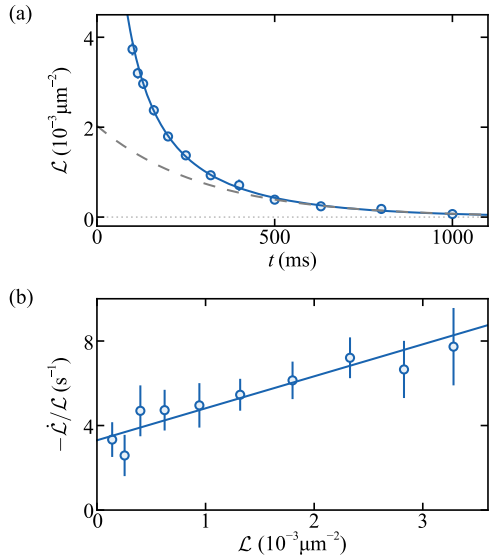


FIG. 5. Quantifying the decay of vortex lines. (a) The evolution of the vortex-line-length density $\mathcal{L}$ [82]. The dashed line shows an exponential fit, corresponding to one-body vortex decay, to data with $t \geq 500$ ms. The faster initial decay hints at vortex-vortex interactions. The solid line shows a fit based on Eq. (4), with $B = 1.0(2)\hbar/m$ and $\tau = 300(40)$ ms. (b) By extracting $\dot{\mathcal{L}} \equiv \mathrm{d}\mathcal{L}/\mathrm{d}t$ at different times during the relaxation, we explicitly recover Eq. (3), with consistent $B = 0.9(2)\hbar/m$ and $\tau = 300(50)$ ms, respectively, the slope and inverse intercept of the solid line.

$$\mathcal{L} = \frac{1}{B\tau\left[\exp\left(\frac{t-t^*}{\tau}\right) - 1\right]}, \tag{4}$$

where t^* is the integration constant.

The solid line in Fig. 5(a) shows a fit based on Eq. (4). We find excellent agreement with the data, with $B = 1.0(2)\hbar/m$. Moreover, by numerically differentiating $\mathcal{L}(t)$, in Fig. 5(b), we recover Eq. (3), with a consistent $B = 0.9(2)\hbar/m$ (the slope of the solid line).

Finally, in Fig. 6, we generalize our study to different a (set at $t = 0$). In Fig. 6(a), we show for three different a values (the $430a_0$ data being the same as in Fig. 5) that $\mathcal{L}(t)$ is always fit well using Eq. (4) with the same $B = 1.0(1)\hbar/m$. Note that here the three curves are offset from each other because (only) the t^* values are different for different a; for weaker interactions, the system takes longer to develop well-defined vortices, but then evolves in an interaction-independent way (see also Refs. [50,84]).

In Fig. 6(b), we collapse all the data from Fig. 6(a) by plotting them according to Eq. (4) with a-dependent t^*; the solid line corresponds to $B = 1.0\hbar/m$. The dashed line shows an exponential with timescale 300 ms [as in Fig. 5(a)], and the horizontal dotted line corresponds to (on average) just one vortex line being present in the whole box trap [see Eq. (2)].

Accounting for the difference in the particle mass, our B is similar to that observed in superfluid ^{4}He in the low-temperature regime, where $B \sim \hbar/m_{\mathrm{He}}$ [13,14,69], despite the large differences between the microscopics of the two systems (even in equilibrium) and the fact that in our case the typical ratio of the vortex-line separation $\mathcal{L}^{-1/2}$ and the vortex-core size is smaller by about 5 orders of magnitude. Numerical simulations of the Gross-Pitaevskii equation also give $B \sim \hbar/m$ [28,29] (see also Refs. [85–87]).

In conclusion, we have observed random vortex lines during far-from-equilibrium Bose-Einstein condensation in an isolated homogeneous 3D gas and shown their decay to be consistent with Vinen turbulence. We observe well-defined vortices and their universal decay in the regime of gas relaxation when the coherence length is already much larger than the vortex-core size; in the future, it would be interesting to also study the earlier stages of relaxation and the expected transition from wave to vortex-dominated turbulence [4]. It would also be interesting to increase the

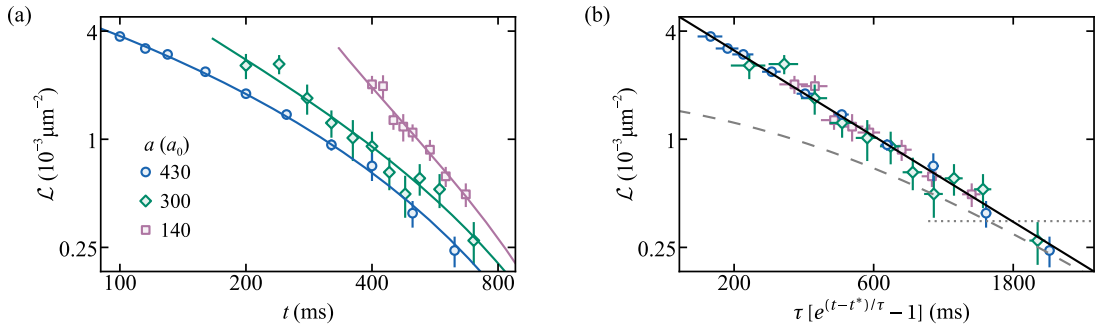


FIG. 6. Universality of Vinen turbulence, for varying a (set at $t = 0$). (a) The evolution of $\mathcal{L}$ for different a is always fit well (solid lines) by Eq. (4), with only the nonuniversal t^* depending on a. Here, all three datasets are fit with the same $B = 1.0(1)\hbar/m$; fitting them independently gives consistent B values. Accounting for the difference in the particle mass, this value of B is essentially the same as obtained for superfluid helium [69]. (b) Plotting the same data according to Eq. (4), with a-dependent t^*, collapses them onto the same universal curve; the solid line corresponds to $B = 1.0\hbar/m$. The dashed line shows the exponential with timescale 300 ms that coincides with the solid line at long times. The horizontal dotted line, $\mathcal{L} = 3.5 \times 10^{-4}$ μm^{-2}, corresponds to (on average) just one vortex line being present in our whole box trap; at smaller $\mathcal{L}$, the dynamics are captured by the one-body exponential decay.

energy per particle, such that the equilibrium temperature is close to the critical temperature for condensation, and study how this affects the vortex-relaxation dynamics. Finally, imaging multiple slices of the same cloud would allow tomography of vortex tangles and studies of their structural dynamics.

Acknowledgments—We thank Gevorg Martirosyan, Jiří Etrych, Nikolai Maslov, Carlo Barenghi, and Mike Gunn for discussions. This work was supported by ERC (UniFlat), EPSRC (Grant No. EP/Y01510X/1), and STFC (Grants No. ST/T006056/1 and No. ST/Y004469/1). Z. H. acknowledges support from the Royal Society Wolfson Fellowship.

Data availability—The data that support the findings of this article are openly available [88].

[1] L. D. Landau, The theory of superfluidity of helium II, J. Phys. (USSR) **5**, 71 (1941).
[2] L. Onsager, Statistical hydrodynamics, Nuovo Cimento **6**, 279 (1949).
[3] R. P. Feynman, Application of quantum mechanics to liquid helium, in *Progress in Low Temperature Physics*, edited by C. J. Gorter (North-Holland Publishing Co., Amsterdam, 1955), pp. 17–53.
[4] B. V. Svistunov, E. S. Babaev, and N. V. Prokof'ev, *Superfluid States of Matter* (CRC Press, Boca Raton, Florida 2015).
[5] W. F. Vinen, Mutual friction in a heat current in liquid helium II I. Experiments on steady heat currents, Proc. R. Soc. A **240**, 114 (1957).
[6] W. F. Vinen, Mutual friction in a heat current in liquid helium II III. Theory of the mutual friction, Proc. R. Soc. A **242**, 493 (1957).
[7] P. W. Anderson and N. Itoh, Pulsar glitches and restlessness as a hard superfluidity phenomenon, Nature (London) **256**, 25 (1975).
[8] T. W. B. Kibble, Topology of cosmic domains and strings, J. Phys. A **9**, 1387 (1976).
[9] W. H. Zurek, Cosmological experiments in superfluid helium?, Nature (London) **317**, 505 (1985).
[10] G. Blatter, M. V. Feigel'man, V. B. Geshkenbein, A. I. Larkin, and V. M. Vinokur, Vortices in high-temperature superconductors, Rev. Mod. Phys. **66**, 1125 (1994).
[11] A. Bulgac, Y.-L. Luo, P. Magierski, K. J. Roche, and Y. Yu, Real-time dynamics of quantized vortices in a unitary Fermi superfluid, Science **332**, 1288 (2011).
[12] J. T. Tough, Superfluid turbulence, in *Progress in Low Temperature Physics*, edited by D. F. Brewer (Elsevier, New York, 1982), Chap. 3, Vol. 8, pp. 133–219.
[13] W. F. Vinen and J. J. Niemela, Quantum turbulence, J. Low Temp. Phys. **128**, 167 (2002).
[14] W. F. Vinen, Quantum turbulence: Achievements and challenges, J. Low Temp. Phys. **161**, 419 (2010).
[15] L. Skrbek, D. Schmoranzer, Š. Midlik, and K. R. Sreenivasan, Phenomenology of quantum turbulence in superfluid helium, Proc. Natl. Acad. Sci. U.S.A. **118**, e2018406118 (2021).
[16] C. F. Barenghi, L. Skrbek, and K. R. Sreenivasan, *Quantum Turbulence* (Cambridge University Press, Cambridge, England, 2023).
[17] A. L. Gaunt, T. F. Schmidutz, I. Gotlibovych, R. P. Smith, and Z. Hadzibabic, Bose-Einstein condensation of atoms in a uniform potential, Phys. Rev. Lett. **110**, 200406 (2013).
[18] C. Eigen, A. L. Gaunt, A. Suleymanzade, N. Navon, Z. Hadzibabic, and R. P. Smith, Observation of weak collapse in a Bose–Einstein condensate, Phys. Rev. X **6**, 041058 (2016).
[19] P. A. Murthy, D. Kedar, T. Lompe, M. Neidig, M. G. Ries, A. N. Wenz, G. Zürn, and S. Jochim, Matter-wave Fourier optics with a strongly interacting two-dimensional Fermi gas, Phys. Rev. A **90**, 043611 (2014).
[20] L. Asteria, H. P. Zahn, M. N. Kosch, K. Sengstock, and C. Weitenberg, Quantum gas magnifier for sub-lattice-resolved imaging of 3D quantum systems, Nature (London) **599**, 571 (2021).
[21] S. Brandstetter, C. Heintze, P. Hill, P. M. Preiss, M. Gałka, and S. Jochim, Magnifying the wave function of interacting fermionic atoms, Phys. Rev. Lett. **135**, 103401 (2025).
[22] M. R. Andrews, C. G. Townsend, H.-J. Miesner, D. S. Durfee, D. M. Kurn, and W. Ketterle, Observation of interference between two Bose condensates, Science **275**, 637 (1997).
[23] A. L. Fetter and A. A. Svidzinsky, Vortices in a trapped dilute Bose–Einstein condensate, J. Phys. Condens. Matter **13**, R135 (2001).
[24] B. V. Svistunov, Highly nonequilibrium Bose condensation in a weakly interacting gas, J. Mosc. Phys. Soc. **1**, 373 (1991).
[25] B. V. Svistunov, Superfluid turbulence in the low-temperature limit, Phys. Rev. B **52**, 3647 (1995).
[26] N. G. Berloff and B. V. Svistunov, Scenario of strongly nonequilibrated Bose-Einstein condensation, Phys. Rev. A **66**, 013603 (2002).
[27] B. Nowak, J. Schole, D. Sexty, and T. Gasenzer, Nonthermal fixed points, vortex statistics, and superfluid turbulence in an ultracold Bose gas, Phys. Rev. A **85**, 043627 (2012).
[28] G. W. Stagg, N. G. Parker, and C. F. Barenghi, Ultraquantum turbulence in a quenched homogeneous Bose gas, Phys. Rev. A **94**, 053632 (2016).
[29] A. Villois, D. Proment, and G. Krstulovic, Evolution of a superfluid vortex filament tangle driven by the Gross–Pitaevskii equation, Phys. Rev. E **93**, 061103(R) (2016).
[30] V. Noel, T. Gasenzer, and K. Boguslavski, Kelvin waves in nonequilibrium universal dynamics of relativistic scalar field theories, Phys. Rev. Res. **7**, 033220 (2025).
[31] G. P. Bewley, D. P. Lathrop, and K. R. Sreenivasan, Visualization of quantized vortices, Nature (London) **441**, 588 (2006).
[32] M. S. Paoletti, M. E. Fisher, K. R. Sreenivasan, and D. P. Lathrop, Velocity statistics distinguish quantum turbulence from classical turbulence, Phys. Rev. Lett. **101**, 154501 (2008).
[33] Y. Tang, W. Guo, H. Kobayashi, S. Yui, M. Tsubota, and T. Kanai, Imaging quantized vortex rings in superfluid helium to evaluate quantum dissipation, Nat. Commun. **14**, 2941 (2023).

[34] C. Peretti, J. Vessaire, É. Durozoy, and M. Gibert, Direct visualization of the quantum vortex lattice structure, oscillations, and destabilization in rotating ^{4}He, Sci. Adv. **9**, eadh2899 (2023).
[35] E. A. L. Henn, J. A. Seman, G. Roati, K. M. F. Magalhães, and V. S. Bagnato, Emergence of turbulence in an oscillating Bose–Einstein condensate, Phys. Rev. Lett. **103**, 045301 (2009).
[36] K. J. Thompson, G. G. Bagnato, G. D. Telles, M. A. Caracanhas, F. E. A. dos Santos, and V. S. Bagnato, Evidence of power law behavior in the momentum distribution of a turbulent trapped Bose-Einstein condensate, Laser Phys. Lett. **11**, 015501 (2013).
[37] W. J. Kwon, G. Moon, J. Y. Choi, S. W. Seo, and Y. I. Shin, Relaxation of superfluid turbulence in highly oblate Bose-Einstein condensates, Phys. Rev. A **90**, 063627 (2014).
[38] N. Navon, A. L. Gaunt, R. P. Smith, and Z. Hadzibabic, Emergence of a turbulent cascade in a quantum gas, Nature (London) **539**, 72 (2016).
[39] S. W. Seo, B. Ko, J. H. Kim, and Y. Shin, Observation of vortex-antivortex pairing in decaying 2D turbulence of a superfluid gas, Sci. Rep. **7**, 4587 (2017).
[40] G. Gauthier, M. T. Reeves, X. Yu, A. S. Bradley, M. A. Baker, T. A. Bell, H. Rubinsztein-Dunlop, M. J. Davis, and T. W. Neely, Giant vortex clusters in a two-dimensional quantum fluid, Science **364**, 1264 (2019).
[41] S. P. Johnstone, A. J. Groszek, P. T. Starkey, C. J. Billington, T. P. Simula, and K. Helmerson, Evolution of large-scale flow from turbulence in a two-dimensional superfluid, Science **364**, 1267 (2019).
[42] N. Navon, C. Eigen, J. Zhang, R. Lopes, A. L. Gaunt, K. Fujimoto, M. Tsubota, R. P. Smith, and Z. Hadzibabic, Synthetic dissipation and cascade fluxes in a turbulent quantum gas, Science **366**, 382 (2019).
[43] X.-P. Liu, X.-C. Yao, Y. Deng, X.-Q. Wang, Y.-X. Wang, C.-J. Huang, X. Li, Y.-A. Chen, and J.-W. Pan, Universal dynamical scaling of quasi-two-dimensional vortices in a strongly interacting fermionic superfluid, Phys. Rev. Lett. **126**, 185302 (2021).
[44] M. Gałka, P. Christodoulou, M. Gazo, A. Karailiev, N. Dogra, J. Schmitt, and Z. Hadzibabic, Emergence of isotropy and dynamic scaling in 2D wave turbulence in a homogeneous Bose gas, Phys. Rev. Lett. **129**, 190402 (2022).
[45] L. H. Dogra, G. Martirosyan, T. A. Hilker, J. A. P. Glidden, J. Etrych, A. Cao, C. Eigen, R. P. Smith, and Z. Hadzibabic, Universal equation of state for wave turbulence in a quantum gas, Nature (London) **620**, 521 (2023).
[46] J. Kim, J. Jung, J. Lee, D. Hong, and Y. Shin, Chaos-assisted turbulence in spinor Bose-Einstein condensates, Phys. Rev. Res. **6**, L032030 (2024).
[47] A. Karailiev, M. Gazo, M. Gałka, C. Eigen, T. Satoor, and Z. Hadzibabic, Observation of an inverse turbulent-wave cascade in a driven quantum gas, Phys. Rev. Lett. **133**, 243402 (2024).
[48] M. Zhao, J. Tao, and I. B. Spielman, Kolmogorov scaling in turbulent 2D Bose-Einstein condensates, Phys. Rev. Lett. **134**, 083402 (2025).
[49] M. Gazo, A. Karailiev, T. Satoor, C. Eigen, M. Gałka, and Z. Hadzibabic, Universal coarsening in a homogeneous two-dimensional Bose gas, Science **389**, 802 (2025).
[50] G. Martirosyan, M. Gazo, J. Etrych, S. M. Fischer, S. J. Morris, C. J. Ho, C. Eigen, and Z. Hadzibabic, A universal speed limit for spreading of coherence, Nature (London) **647**, 608 (2025).
[51] Y. Jiang, N. Maslov, A. Karailiev, C. Eigen, M. Gazo, and Z. Hadzibabic, A nonequilibrium equation of state for a turbulent 2D Bose gas, arXiv:2602.06131.
[52] M. R. Matthews, B. P. Anderson, P. C. Haljan, D. S. Hall, C. E. Wieman, and E. A. Cornell, Vortices in a Bose-Einstein condensate, Phys. Rev. Lett. **83**, 2498 (1999).
[53] K. W. Madison, F. Chevy, W. Wohlleben, and J. Dalibard, Vortex formation in a stirred Bose-Einstein condensate, Phys. Rev. Lett. **84**, 806 (2000).
[54] J. R. Abo-Shaeer, C. Raman, J. M. Vogels, and W. Ketterle, Observation of vortex lattices in Bose-Einstein condensates, Science **292**, 476 (2001).
[55] V. Bretin, P. Rosenbusch, F. Chevy, G. V. Shlyapnikov, and J. Dalibard, Quadrupole oscillation of a single-vortex Bose-Einstein condensate: Evidence for Kelvin modes, Phys. Rev. Lett. **90**, 100403 (2003).
[56] M. W. Zwierlein, J. R. Abo-Shaeer, A. Schirotzek, C. H. Schunck, and W. Ketterle, Vortices and superfluidity in a strongly interacting Fermi gas, Nature (London) **435**, 1047 (2005).
[57] C. N. Weiler, T. W. Neely, D. R. Scherer, A. S. Bradley, M. J. Davis, and B. P. Anderson, Spontaneous vortices in the formation of Bose-Einstein condensates, Nature (London) **455**, 948 (2008).
[58] D. V. Freilich, D. M. Bianchi, A. M. Kaufman, T. K. Langin, and D. S. Hall, Real-time dynamics of single vortex lines and vortex dipoles in a Bose-Einstein condensate, Science **329**, 1182 (2010).
[59] T. W. Neely, E. C. Samson, A. S. Bradley, M. J. Davis, and B. P. Anderson, Observation of vortex dipoles in an oblate Bose-Einstein condensate, Phys. Rev. Lett. **104**, 160401 (2010).
[60] Mark J. H. Ku, W. Ji, B. Mukherjee, E. Guardado-Sanchez, L. W. Cheuk, T. Yefsah, and M. W. Zwierlein, Motion of a solitonic vortex in the BEC–BCS crossover, Phys. Rev. Lett. **113**, 065301 (2014).
[61] S. Donadello, S. Serafini, M. Tylutki, L. P. Pitaevskii, F. Dalfovo, G. Lamporesi, and G. Ferrari, Observation of solitonic vortices in Bose-Einstein condensates, Phys. Rev. Lett. **113**, 065302 (2014).
[62] S. Serafini, M. Barbiero, M. Debortoli, S. Donadello, F. Larcher, F. Dalfovo, G. Lamporesi, and G. Ferrari, Dynamics and interaction of vortex lines in an elongated Bose-Einstein condensate, Phys. Rev. Lett. **115**, 170402 (2015).
[63] W. J. Kwon, G. Del Pace, K. Xhani, L. Galantucci, A. Muzi Falconi, M. Inguscio, F. Scazza, and G. Roati, Sound emission and annihilations in a programmable quantum vortex collider, Nature (London) **600**, 64 (2021).
[64] R. J. Fletcher, A. Shaffer, C. C. Wilson, P. B. Patel, Z. Yan, V. Crépel, B. Mukherjee, and M. W. Zwierlein, Geometric squeezing into the lowest Landau level, Science **372**, 1318 (2021).
[65] R. H. Kraichnan, Condensate turbulence in a weakly coupled boson gas, Phys. Rev. Lett. **18**, 202 (1967).
[66] A. Piñeiro Orioli, K. Boguslavski, and J. Berges, Universal self-similar dynamics of relativistic and nonrelativistic field

theories near nonthermal fixed points, Phys. Rev. D **92**, 025041 (2015).
[67] I. Chantesana, A. P. Orioli, and T. Gasenzer, Kinetic theory of nonthermal fixed points in a Bose gas, Phys. Rev. A **99**, 043620 (2019).
[68] V. Rosenhaus and G. Falkovich, Weak and strong turbulence in self-focusing and defocusing media, arXiv:2501.12451.
[69] P. M. Walmsley and A. I. Golov, Quantum and quasiclassical types of superfluid turbulence, Phys. Rev. Lett. **100**, 245301 (2008).
[70] G. Martirosyan, C. J. Ho, J. Etrych, Y. Zhang, A. Cao, Z. Hadzibabic, and C. Eigen, Observation of subdiffusive dynamic scaling in a driven and disordered Bose gas, Phys. Rev. Lett. **132**, 113401 (2024).
[71] J. Etrych, G. Martirosyan, A. Cao, Jake A. P. Glidden, L. H. Dogra, J. M. Hutson, Z. Hadzibabic, and C. Eigen, Pinpointing Feshbach resonances and testing Efimov universalities in ^{39}K, Phys. Rev. Res. **5**, 013174 (2023).
[72] See End Matter for details on our initial state.
[73] I. Shvarchuck, C. Buggle, D. S. Petrov, K. Dieckmann, M. Zielonkovski, M. Kemmann, T. G. Tiecke, W. von Klitzing, G. V. Shlyapnikov, and J. T. M. Walraven, Bose-Einstein condensation into nonequilibrium states studied by condensate focusing, Phys. Rev. Lett. **89**, 270404 (2002).
[74] S. Tung, G. Lamporesi, D. Lobser, L. Xia, and E. A. Cornell, Observation of the presuperfluid regime in a two-dimensional Bose gas, Phys. Rev. Lett. **105**, 230408 (2010).
[75] R. J. Fletcher, M. Robert-de-Saint-Vincent, J. Man, N. Navon, R. P. Smith, K. G. H. Viebahn, and Z. Hadzibabic, Connecting Berezinskii–Kosterlitz–Thouless and BEC phase transitions by tuning interactions in a trapped gas, Phys. Rev. Lett. **114**, 255302 (2015).
[76] We use a red-detuned laser beam to realize a harmonic trap, with frequencies $\omega_x \approx 2\pi \times 40$ Hz, $\omega_y \approx 2\pi \times 45$ Hz, and $\omega_z \approx 0$. The slight anisotropy in the x-y plane limits our resolution to a distance that corresponds to ≈2 μm *in situ*.
[77] We use a laser beam shaped by a digital micromirror device to optically pump only a slice of the cloud into the highest hyperfine ground state and then image only the atoms in that state.
[78] D. J. Tritton, *Physical Fluid Dynamics* (Springer Science & Business Media, New York, 2012).
[79] T. Binzoni, E. Dumonteil, and A. Mazzolo, Universal property of random trajectories in bounded domains, Phys. Rev. E **112**, 044105 (2025).
[80] For the data in Figs. 4 and 5, we count imprints in our images within a central circle of radius $r_D \approx 52$ μm, which corresponds to *in situ* $S \approx 2800$ μm^2. None of our results change (within error bars) if we reduce r_D to ≈34 μm, which corresponds to $S \approx 1500$ μm^2.
[81] We exclude clusters with fewer pixels than $N_{\min} = 4$, which is sufficiently large to avoid counting noise, so N_i vanishes for $t \to \infty$; see End Matter for examples of our counting.
[82] In both Figs. 5 and 6, we use the calibrated conversion (the average N_i/A, see Fig. 4) to extract $\mathcal{L}$ from A. Directly using Eq. (2) does not change our results within statistical errors.
[83] K. W. Schwarz, Three-dimensional vortex dynamics in superfluid ^{4}He: Line-line and line-boundary interactions, Phys. Rev. B **31**, 5782 (1985).
[84] S. M. Fischer, M. Gazo, S. J. Morris, N. Maslov, H. Zhang, J. Etrych, G. Martirosyan, C. Eigen, and Z. Hadzibabic, Weak wave turbulence as a precursor to universal coarsening in a homogeneous Bose gas, arXiv:2605.22906.
[85] M. Tsubota, T. Araki, and S. K. Nemirovskii, Dynamics of vortex tangle without mutual friction in superfluid ^{4}He, Phys. Rev. B **62**, 11751 (2000).
[86] A. W. Baggaley, L. K. Sherwin, C. F. Barenghi, and Y. A. Sergeev, Thermally and mechanically driven quantum turbulence in helium II, Phys. Rev. B **86**, 104501 (2012).
[87] V. Shukla, P. D. Mininni, G. Krstulovic, P. C. di Leoni, and M. E. Brachet, Quantitative estimation of effective viscosity in quantum turbulence, Phys. Rev. A **99**, 043605 (2019).
[88] 10.17863/CAM.134385.

End Matter

Initial state—To prepare our far-from-equilibrium initial state, we follow Ref. [70]. We start with a quasipure condensate, turn off the interactions, and drive the noninteracting gas for ≈1 s along the box axis using a time-varying force $F\cos(\omega_s t)$, where $\omega_s/(2\pi) = 10$ Hz and $F/m \approx 0.1$ m s^{-2}, created by a magnetic field gradient. In the absence of interactions, weak optical disorder within the box scatters the atoms into transverse directions, so once we stop driving and wait for ≈1 s, the state is essentially isotropic. Our linear driving does not introduce angular momentum into the gas, and the isotropic initial state has no net vorticity or any other large-scale flow.

In Fig. 7, we plot the spectral population density, $N_k = 4\pi k^2 n_k$, of our initial state, where k is the wave number and n_k the momentum distribution, normalized

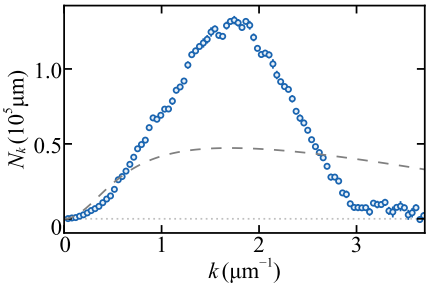


FIG. 7. The spectral population density, $N_k = 4\pi k^2 n_k$, in our initial state; here k is the wave number and n_k the momentum distribution, normalized such that $\int N_k dk = N$. For comparison, the dashed line shows the thermal (equilibrium) Bose distribution with the same N and the same position of the peak of N_k, at $k_p \approx 1.7$ μm^{-1}.

such that $\int N_k \mathrm{d}k = N$, where N is the total atom number. The N_k has a peak at $k_\mathrm{p} \approx 1.7\ \mu\mathrm{m}^{-1}$, corresponding to fluctuations at a length scale $\sim 1/k_\mathrm{p} \approx 0.6\ \mu\mathrm{m}$, and no large-scale coherence; this length scale is smaller than the equilibrium vortex-core size for all our values of the scattering length a during the gas relaxation (see also Ref. [84]).

While the gas in this initial state has essentially no coherence, the energy per particle is very low, so during relaxation a significant condensate emerges, and well-defined vortices are observed once most particles are at $k < 1/\xi$. For reference, in Fig. 7 we also show, with a dashed line, the thermal (equilibrium) Bose distribution with the same k_p and N; compared to this state, our far-from-equilibrium initial state has essentially no high-k tails and has about 4 times lower energy.

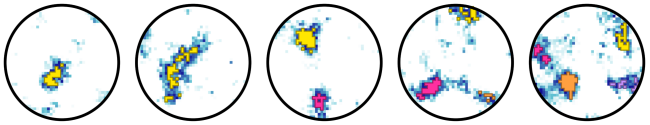


FIG. 8. Cluster examples. Each image shows our detection region of radius $r_\mathrm{D} = 52\ \mu\mathrm{m}$. Within each image, each distinct cluster is indicated by a different color. The detected clusters are overlaid on the experimental images with the color scale as in Fig. 3.

Examples of counted clusters—In Fig. 8, we show examples of the counted clusters of pixels corresponding to distinct vortex imprints.